Available online at www.sciencedirect.com
ScienceDirect
Journal of Molecular Catalysis A: Chemical 264 (2007) 299–308
JOURNAL OF MOLECULAR CATALYSIS A: CHEMICAL
www.elsevier.com/locate/molcata

First-principles calculations of CH_4 dissociation on Ni(1 0 0) surface along different reaction pathways

Yi-An Zhu [a,*], Ying-Chun Dai [a], De Chen [b], Wei-Kang Yuan [a,*]

[a] *UNILAB, State Key Laboratory of Chemical Reaction Engineering, East China University of Science and Technology, Shanghai 200237, PR China*
[b] *Department of Chemical Engineering, Norwegian University of Science and Technology (NTNU), N-7491 Trondheim, Norway*

Received 22 August 2006; received in revised form 20 September 2006; accepted 21 September 2006
Available online 29 September 2006

Abstract

First-principles calculations based on density functional theory and the generalized gradient approximation have been used to study the adsorption and dissociation of CH_4 on Ni(1 0 0) surface. The favored adsorption sites of H, CH_3, and CH_4 are identified by considering the energy and stability of various binding sites. H atoms prefer the fourfold Hollow sites, while CH_3 species favors the Bridge site with one of the C–H bonds pointing towards the neighbor Ni atom. When H and CH_3 are coadsorbed on Ni(1 0 0) surface, several stable configurations are found, in which the atomic H and CH_3 species are adsorbed at the Hollow and Bridge site, respectively, because of their little energetic difference. Through the electronic and vibrational calculations, the C–H–Ni three-center bond is regarded as the key factor determining the CH_3 adsorption. The CH_4 dissociation on Ni(1 0 0) surface is investigated with three different CH_4 orientations considered. The energy barriers are calculated to be 0.61, 0.61 and 0.62 eV, corresponding to the CH_4 molecules orientated with one, two and three C–H bonds pointing towards the surface, respectively. All calculated activation energies have been corrected by including zero-point energy and dispersion energy, and are in good agreement with the experimental result (0.61 ± 0.02 eV). Because the energy barriers for the different reaction pathways take similar values, the CH_4 orientation has a minor effect on the reactivity.

Keywords: Density functional theory; Chemisorption; Methane; Nickel

1. Introduction

The dissociation of methane on nickel surfaces to form surface-bound methyl and hydrogen is of great importance as the important step in steam reforming process which converts natural gas to a mixture of monoxide carbon and hydrogen [1]. Furthermore, in the past 20 years, this reaction is also regarded as the starting point for synthesis of carbon nanotubes (CNTs) and carbon nanofibers (CNFs) by chemical vapor deposition (CVD) [2,3]. Owing to the industrial background and important applications, much experimental as well as theoretical work has been devoted to an understanding of the adsorption and dissociation of methane on nickel surfaces [4–22]. However, this process is such a complex multidimensional dynamical reaction that its microscopic description remains controversial [4].

Yang and Chen performed both experimental and theoretical studies on carbon filament growth to verify that the Ni(1 0 0) and Ni(1 1 0) surfaces were among the gas/metal interface, while the Ni(1 1 1) and Ni(3 1 1) surfaces were among the graphite/metal interface [5]. Furthermore, the most reliable measurement of the activation energy barrier for CH_4 dissociative adsorption on Ni(1 0 0) surface gave a value of 0.61 eV [6], much lower that that on Ni(1 1 1) surface (0.77 eV) [7]. Therefore, Ni(1 0 0) surface plays a key role in decomposition of carbon-containing gases. Through molecular beam experiments [8–10], it was found that CH_4 chemisorption was a direct process that could be activated by both incident kinetic energy normal to the surface and thermal vibrational energy of the incident CH_4. Two models were proposed to explain the experimental data. Luntz and Harris believed that the CH_4 dissociation on metal surfaces was a direct dynamical process [4], while Ukraintsev and Harrison claimed a statistical model [11]. Beck et al. performed quantum state-resolved experiments to prove the CH_4 dissociation on Ni(1 0 0) surface was a vibrational mode-specific gas–surface reaction and the C–H bond stretch had a substantial projection on the

* Corresponding authors. Tel.: +86 21 6425 2884; fax: +86 21 6425 3528.
E-mail addresses: yanzhu@ecust.edu.cn (Y.-A. Zhu), wkyuan@ecust.edu.cn (W.-K. Yuan).

1381-1169/$ – see front matter © 2006 Elsevier B.V. All rights reserved.
doi:10.1016/j.molcata.2006.09.043

reaction coordinate [12]. Recently, they found the reactivity of the symmetric-stretch excited CH_4 was about an order of magnitude higher than that of the CH_4 excited to the asymmetric stretch [13]. Juurlink et al. used the same experimental method to find that despite the enhancement of the asymmetric C–H stretching eigenstate in promoting CH_4 dissociation, transitional energy was more effective [14]. They also reported that both C–H stretching and bending vibrations contributed significantly to activation in CH_4 dissociation, but the stretch coordinate was more effective than the bending state at moving reagents toward the transition state [15].

Wave packet simulations performed by Milot and Jansen showed that the initial vibrational excitations of the symmetric stretch mode gave the highest enhancement of the CH_4 dissociation probability if the dissociation occurred primarily in the orientation with multiple bonds pointing towards the surface [16]. A three-parameter microcanonical analysis was performed by Abbott et al., indicating an apparent threshold energy for C–H bond cleavage of CH_4 incident on Ni(1 0 0) surface of 0.67 eV [17]. In early first-principles calculations, Ni(1 0 0) surface has been represented either with a small cluster or by using a periodic slab. Ab initio quantum chemistry calculations performed by Swang et al. indicated that the activation energy for CH_4 chemisorption on Ni(1 0 0) surface was in the range of 0.69 ± 0.04 eV using a cluster model [18]. Bengaard et al. conducted self-consistent density functional theory (DFT) calculations to gain an energy barrier of 1.19 eV [19], in which the slab was kept rigid to reduce computational effort. More recently, Lai et al. proposed activation energies of 0.64 and 0.73 eV without and with spin-polarization, respectively [20], through a first-principles study. In their study, the energy barrier was initially evaluated without spin-polarization effect and the spin-polarized results were obtained by using the single point spin-polarized calculations.

In the present paper, we perform first-principles density functional theory calculations to investigate the CH_4 dissociative adsorption on Ni(1 0 0) surface starting from three different CH_4 orientations. Our paper is organized as follows. In Section 2, the details of our computational methods are described. The calculated binding energies and diffusion energy barriers are given in Section 3. These computational results are compared with previous experimental and theoretical data to examine the accuracy of our method. In Section 4, we conclude by discussing the implication of our results for understanding the effect of the CH_4 orientation on energy barriers for the CH_4 dissociation.

2. Computational details

First-principles calculations based on DFT are performed by using a plane-wave pseudopotential (PW-PP) method [23–25], in which the electronic wavefunctions at each *k*-point in periodic systems are written as a product of a wavelike part and a cell periodic part, the latter being expanded using a plane wave basis set. The interactions between valence electrons and ion cores are represented by Blöchl's all-electron-like projector augmented wave method (PAW) [26], which regards the 4s 3d states as the valence configuration for Ni, 2s 2p states for C and 1s state for H (we use the standard version of the PAW-GGA potential for Ni and H, and the soft one for C). Exchange and correlation of the Kohn-Sham theory are treated with the generalized gradient approximation functional (GGA) of PW91 [27]. A plane wave energy cut off of 350 eV is used in the present calculation and the total energies in all geometry optimization calculations are converged to within 1 meV/atom successfully. Brillouin zone sampling is performed using a Monkhorst–Pack grid [28] and electronic occupancies are determined according to a Methfessel–Paxton scheme [29] with an energy smearing of 0.1 eV. Because there is a magnetic element (Ni) involved in the system, spin polarized effect has been considered. The calculations performed by Kresse and Hafner showed that surface magnetism was essential for an accurate quantitative description of adsorption energy [30].

The Ni(1 0 0) surface is represented as a five-layer slab with a $p(3 \times 3)$ supercell, corresponding to a CH_4 coverage of 0.11 monolayer (ML). Our model is larger than that used in Ref. [20]. A $p(2 \times 2)$ surface supercell has also been considered, and it is found that this supercell is not large enough to neglect the lateral adsorbate interactions. Therefore, our results are more appropriate to be compared to experimental data with low surface coverages. The bottom two layers of the slab are constrained to their crystal lattice positions. The neighboring slabs are separated by a vacuum layer as large as 12 Å in order to avoid periodic interactions. Another test calculation is made to show that the relaxation of deeper layers has only a very small effect on the surface reaction since the forces on these layers are negligible. The first Brillouin zone of the $p(3 \times 3)$ supercell is sampled with a $2 \times 2 \times 1$ *k*-point mesh which is evidenced to be sufficient for such a large cell [22].

The energies of localized vibrations are substantial for light atoms such as H atoms. It is necessary to make zero-point energy (ZPE) corrections to the adsorption energies and activation energy barriers. Especially at the saddle point, one of the modes has negative curvature so the corresponding contribution to the ZPE is lost, and the energy barrier is consequently lowered. The Hessian matrix for the potential energy surface is calculated using finite difference approximation, and diagonalized to find the normal modes of calculated systems. The adsorbates (CH_3, CH_4) and the metal atoms to which the adsorbates are attached are displaced in the direction of each Cartesian coordinate, while the other Ni atoms are kept rigid during these finite difference calculations because in the preliminary calculation, the CH_4 vibrational frequencies adopt almost the same wavenumbers with and without the relaxation of these metal atoms.

It was reported that nonbonding interactions controlled the CH_4 physisorption on transition metal surfaces [20,31]. However, DFT provides a poor description of van der Waals (vdW) forces and yields repulsive forces only [32–34]. Therefore, the dominant contribution to the long-range intermolecular potential, the dispersion energy, should be added to the DFT calculations. The dispersion energy (E_{disp}) can be written as

$$E_{\text{disp}} = -\frac{C_{6ij}}{r^6} - \frac{C_{8ij}}{r^8} - \frac{C_{10ij}}{r^{10}} - \cdots, \quad (1)$$

where r is the distance between the C atom in CH_4 and Ni surface, and

$$C_{6ij} = \frac{2}{3}\frac{1}{(4\pi\varepsilon_0)^2}\frac{\alpha_i\alpha_j I_i I_j}{I_i + I_j} \quad (2)$$

where α is the electronic polarizability and I is the ionization energy [35]. The higher-order coefficients, C_8, C_{10}, etc. are taken into account by simply increase the C_6 coefficient by 25%. All the coefficients C_6, C_8 and C_{10} are positive, so that the energy contributions are all attractive.

An improved version of the nudged elastic band method, the climbing-image NEB (CI-NEB) [36–38], is used to locate the minimum energy path (MEP) and transition states for CH_4 dissociation. A number of intermediate images are constructed along the reaction path between the energetically favorable reactants and products. With the two endpoints fixed, the intermediates are optimized partially using a velocity quench algorithm [39] followed by a quasi-Newton algorithm. Once a MEP is found, the dimmer method [40] is used to reconverge saddle points. Minima and saddle points are considered converged when the maximum force in every degree of freedom is less than 0.01 eV/Å. In order to obtain accurate forces, the total energy and band structure energy are converged to within 1×10^{-8} eV/atom during the electronic optimization. Such a calculation is computationally demanding because of the high precision and large numbers of ionic relaxation steps for each image along the reaction path.

3. Results and discussion

3.1. H chemisorption on Ni(1 0 0) surface

It was reported that the adsorbed H and CH_3 are the primary products of CH_4 dissociation by electron energy loss spectroscopy (EELS) [41,42]. The sites considered for H adsorption on Ni(1 0 0) surface are as follows (Fig. 1): a hollow fourfold site (Hollow site), a bridge site between two Ni atoms (Bridge site), and an atop site above a single Ni atom (Atop site). The energies and the corresponding geometries of atomic H adsorbed at various sites are examined to find the most favorable configuration. The H adsorption energy (ΔE_{ads}) is defined here as

$$\Delta E_{ads} = E_{H+Ni(1\,0\,0)} - E_H - E_{Ni(1\,0\,0)} \quad (3)$$

The first term on the right hand is the total energy of Ni(1 0 0) surface with an H atom adsorbed; the second term is the total energy of an isolated H atom; the last term is the total energy of clean Ni(1 0 0) surface. The calculated results are summarized in Table 1. The negative sign of the adsorption energy indicates that the H adsorption on Ni(1 0 0) surface is an exothermic process. From the table, the H atoms prefer the Hollow site which is in agreement with experimental measurements by Christmann et al. [43]. This is because the atomic H is coordinated by four Ni atoms at the Hollow site while only two and one Ni atoms at the Bridge and Atop sites, respectively, i.e., higher coordination results in better stability. The most important geometry parameters – the shortest H–Ni distance and the height of the H atom above the surface – are also shown in Table 1.

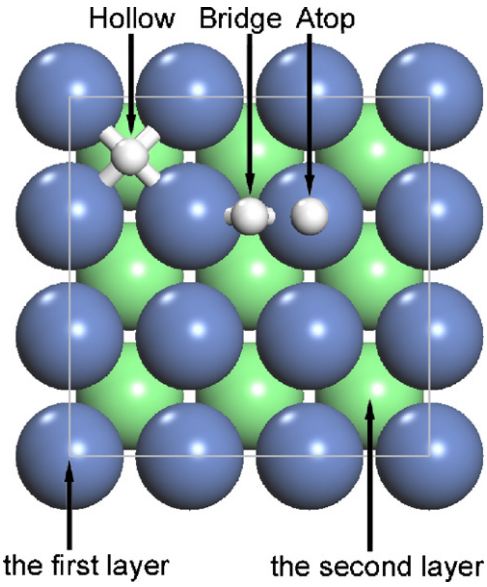

Fig. 1. Schematic representations of H adsorption on three high-symmetry sites of Ni(1 0 0) surface. Small balls denote H atoms. Large balls denote Ni atoms in the first and second layers.

3.2. CH_3 chemisorption and diffusion on Ni(1 0 0) surface

3.2.1. CH_3 chemisorption on Ni(1 0 0) surface

Similar to the atomic H, the CH_3 species is bound to the aforementioned three high-symmetry sites of Ni(1 0 0) surface and two different CH_3 orientations are considered at each site, shown in Fig. 2. At the Hollow and Bridge sites, one of C–H bonds in CH_3 species points toward either a Bridge site (the configurations are named as Hollow1 and Bridge1, respectively) or an Atop site (Hollow2 and Bridge2, respectively). And at the Atop site, one of C–H bonds points toward either a Bridge site (Atop1) or a Hollow site (Atop2). The adsorption energies and optimized geometry parameters are listed in Table 2, and the corrected values are calculated by considering the ZPE correction. Comparing the adsorption energies, one can see that the Bridge2 configuration is preferred, consistent with the previous DFT-GGA study [20]. The valence charge density is calculated as CH_3 species is adsorbed at various sites and plotted perpendicular to the Ni(1 0 0) surface with the Ni–C bond involved (Fig. 3). It is evident that strong covalent C–Ni bonds are formed in all six configurations, and these bonds are seen in the figures as "bridges" of electronic density between C and Ni atoms. At the Atop site, the electronic density between the C and Ni atoms is largest, indicating the strongest Ni–C bond. This also can be

Table 1
Adsorption energies and geometries of H atom on Ni(1 0 0) surface

Site	ΔE_{ads} (eV)	d_{H-Ni}[a] (Å)	$d_{H-surface}$[b] (Å)
Hollow	−2.79	1.836 (4)[c]	0.554
Bridge	−2.68	1.616 (2)	1.080
Atop	−2.23	1.472	1.495

[a] d_{H-Ni} denotes the shortest H–Ni distance.
[b] $d_{H-surface}$ denotes the height of the H atom above the surface.
[c] Numbers in parentheses show the amount of the corresponding value.

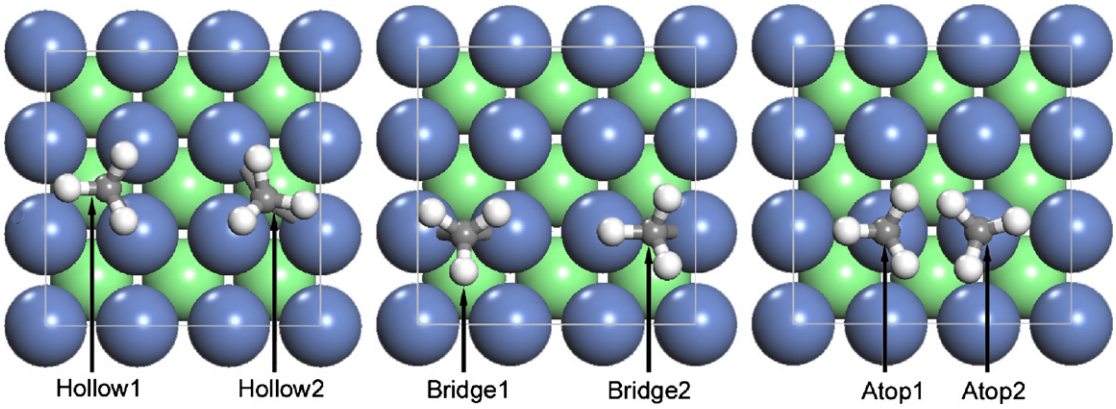

Fig. 2. Schematic representations of CH_3 adsorption geometries on Ni(1 0 0) surface with different orientations. Small white balls denote H atoms. Small grey balls denote C atoms.

deduced from the comparison of $d_{C–Ni}$ in Table 2. The shortest Ni–C bond length at the Atop site strengthens the covalent bond and the underlying Ni atom is moved out normal to the surface by about 0.2 Å. However, the CH_3 adsorption at the Bridge site is more exothermic than that at the Atop site as mentioned above. This is because the interaction between CH_3 and Ni surface is of a strong three-center character [44].

To further investigate the CH_3 chemisorption on Ni(1 0 0) surface by analyzing the electronic structure, local density of states (LDOSs) around C atom are calculated at various adsorption sites, and the results are shown in Fig. 4. The zero energy refers to the Fermi level, and the peaks corresponding to the molecular orbitals of isolated CH_3 are also represented (dashed lines). In Fig. 4, the lowest energy peek refers to the 2a1 orbital which is the lowest occupied valence orbital in CH_3. It is clear that its energy is lowered by about 1 eV as CH_3 is bound to the Hollow and Bridge sites, while at the Atop site, no energy change occurs, indicating there is no interaction between the 2a1 orbital and the metal substrate in this instance. The peak at about 6 eV below the Fermi level is attributed to the state of 1e orbital character. The CH_3 adsorptions at the Hollow and Bridge sites result in an energy decrease of the 1e orbital while the orbital energy is shifted to higher value at the Atop site. This is because the mixing between the 1e and Ni 3d states, in fact, corresponds to a C–H–Ni three-center bond [44] which is discussed in detail below. At the Atop site, the 1e–3d mixing is very weak, arising from a larger H–Ni separation. The 3a1 orbital is the highest occupied molecular orbital. A dramatic orbital mixing of the 3a1 orbital with the metal 3d state upon chemisorption can be seen at all adsorption sites. The mixing results in substantial decreases in energy of the 3a1 orbital by up to 5.6 and 5 eV at the Hollow and Bridge sites, respectively, which are much larger than that at the Atop site (4 eV). The 3a1–3d mixing is weakened and positioned at higher energy at the Atop site because C atom has only one Ni neighbor with which it can mix.

As claimed by Michaelides and Hu [44], the C–H–Ni bond is formed as CH_3 is adsorbed on Ni(1 1 1) surface. They pointed out that the observed mode softening in CH_3 species was attributed to the formation of the three-center bond. Through our vibrational calculations of the CH_3 adsorbed on Ni(1 0 0) surface, the mode softening is also found. For the most stable Bridge2 configuration, the 'soft' frequency of the C–H symmetric stretching occurs at $\sim$2613 cm^{-1}, which corresponds to a red shift of approximate 346 cm^{-1}, compared to the gas-phase C–H symmetric stretching frequency of $\sim$2959 cm^{-1}. This mode soft-

Table 2
Adsorption energies and geometries of CH_3 on Ni(1 0 0) surface

Configuration	ΔE_{ads} (eV)		$d_{C–Ni}$[a] (Å)	$d_{C–surface}$[b] (Å)	$d_{Ni–H}$[c] (Å)	$d_{C–H}$[d] (Å)	∠HCH[e] (°)
	Uncorrected[f]	Corrected[g]					
Hollow1	−1.84	−1.88	2.070 (2)	1.556	2.031 (2)	1.113, 1.120 (2)	105.236, 106.539 (2)
Hollow2	−1.86	−1.91	2.002	1.516	1.923 (2)	1.108, 1.134 (2)	101.995, 105.880 (2)
Bridge1	−1.93	−1.95	2.057 (2)	1.779	2.095 (2)	1.098, 1.115 (2)	103.800, 109.604 (2)
Bridge2	−1.96	−1.98	1.995	1.771	1.838	1.102 (2), 1.138	104.816 (2), 110.748
Atop1	−1.76	−1.76	1.947	2.139	2.524 (2)	1.099, 1.101 (2)	110.058, 110.091 (2)
Atop2	−1.75	−1.75	1.945	2.177	2.521	1.099, 1.101 (2)	110.081, 110.086 (2)

[a] d_{C-Ni} denotes the shortest C–Ni distance.
[b] $d_{C–surface}$ denotes the height of the C atom above the surface.
[c] d_{Ni-H} denotes the shortest Ni–H distance.
[d] $d_{C–H}$ denotes the lengths of C–H bonds in CH_3 species.
[e] ∠HCH denotes the angles between the C–H bonds in CH_3 species.
[f] The uncorrected adsorption energy is calculated as $\Delta E_{ads} = E_{CH_3+Ni(100)} - E_{CH_3} - E_{Ni(100)}$.
[g] The corrected adsorption energy is calculated with the ZPE correction considered.

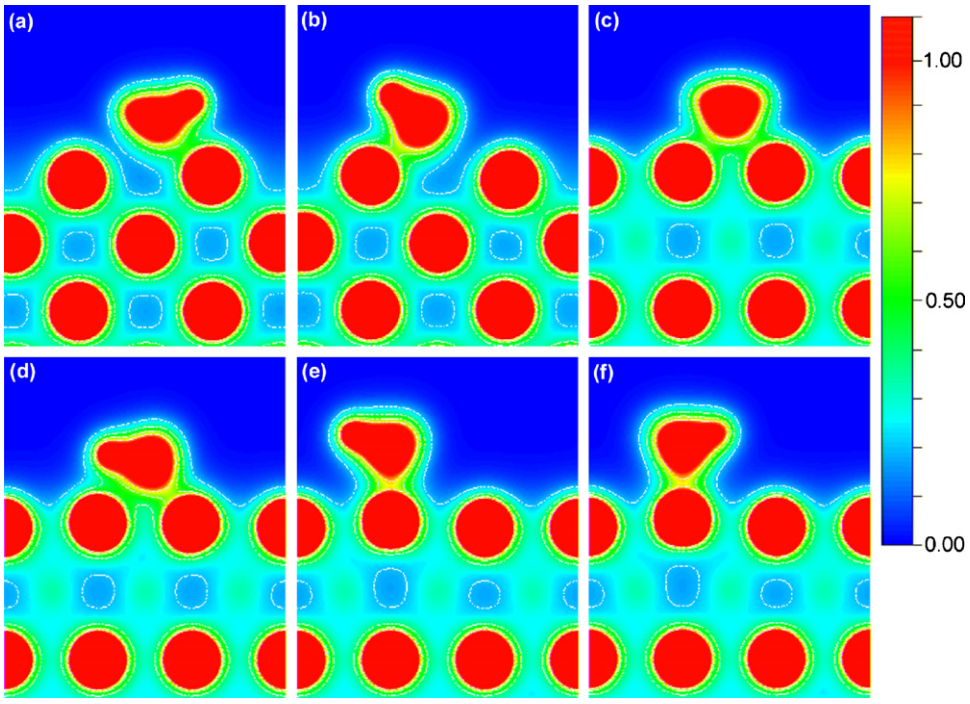

Fig. 3. The valence charge density calculated for different CH_3 adsorption geometries and plotted perpendicular to Ni(1 0 0) surface with the Ni–C bond involved: (a) Hollow1. (b) Hollow2. (c) Bridge1. (d) Bridge2. (e) Atop1. (f) Atop2.

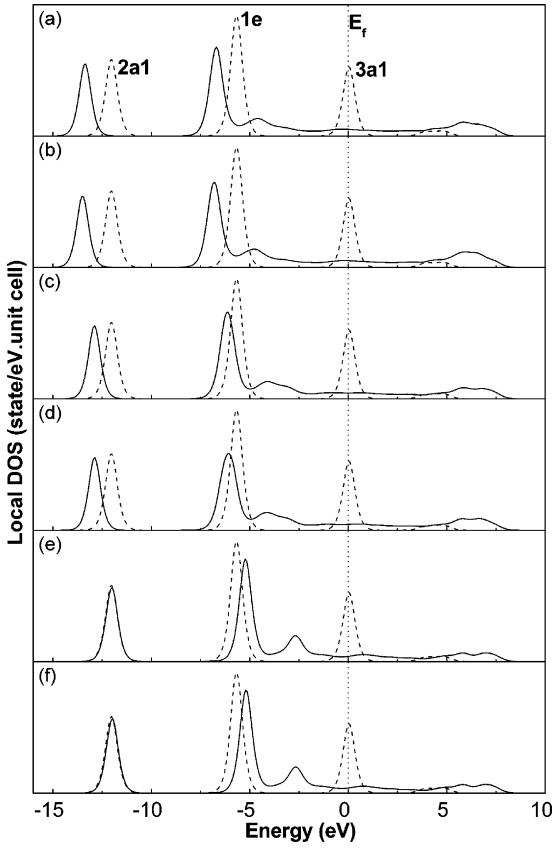

Fig. 4. LDOSs around C atom for various CH_3 adsorption configurations on Ni(1 0 0) surface: (a) Hollow1. (b) Hollow2. (c) Bridge1. (d) Bridge2. (e) Atop1. (f) Atop2. The zero energy refers to the Fermi level. The peaks corresponding to the isolated CH_3 molecular orbitals are also represented as dashed lines.

ening predicts a weakening of the C–H bond. In fact, the C–H bond can be regarded as an electron donor. The electrons in the C–H bond are attracted by the deep Ni 3d potential and delocalized into the region between the three atoms [44]. The formed C–H–Ni bond results in a shortened H–Ni distance and a lengthened C–H bond. In Table 2, the Bridge2 configuration has the longest C–H bond length and the shortest Ni–H distance, achieving the maximum multicenter bonding. Therefore, the Bridge site is more favorable for CH_3 adsorption than the Atop site.

3.2.2. *CH_3 diffusion on Ni(1 0 0) surface*

The strength of the C–H–Ni three-center bond can also be characterized by the energy barrier for CH_3 rotation on Ni surface [44]. Therefore, the CI-NEB method is used to explore the MEP for CH_3 rotation on Ni(1 0 0) surface. In the calculation, both the initial and final states adopt the most stable Bridge2 configuration, and the CH_3 molecule is rotated through ~60° around the surface normal going through the C atom. The calculated MEP is shown in Fig. 5, with the initial state, the transition states, the intermediate and the final state represented. The energy barrier without ZPE correction is ca. 28 meV which is much lower than that for CH_3 rotation on Ni(1 1 1) surface (0.17 eV) [22]. On the Ni(1 1 1) surface, the CH_3 molecule is initially rotated around one H atom from the most stable Fcc site to the Hcp site, and then back to the Fcc site owing to the strong C–H–Ni bond. However, in our calculation, the C atom is located at the Bridge site throughout the rotation. This is also, in fact, because the three-center bond is strongest when CH_3 is located at the Bridge site, and it prevents the CH_3 molecule from diffusing to other adsorption sites.

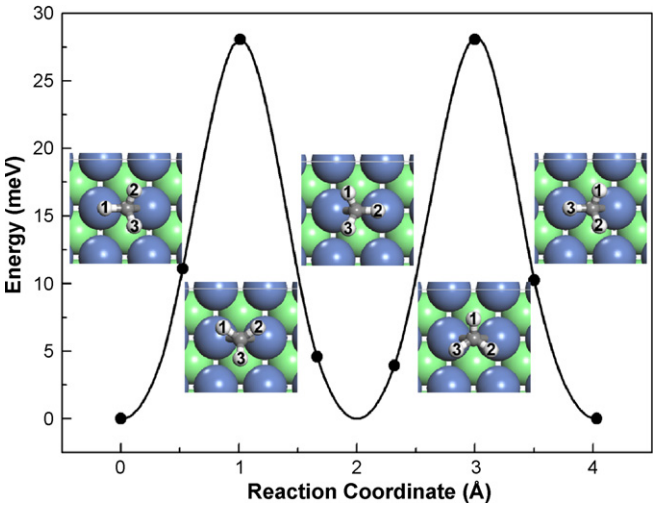

Fig. 5. MEP for CH_3 rotation at the Bridge site. The configurations for the initial state, the transition states, the intermediate and the final state are also represented.

3.3. Coadsorption of H and CH_3 on Ni(1 0 0) surface

The coadsorption of H and CH_3 on Ni(1 0 0) surface is investigated by assigning the atomic H and CH_3 species to different adsorption sites, respectively, and the predicted geometries are illustrated in Fig. 6. The calculated adsorption energies and optimized geometry parameters are summarized in Table 3. As seen from the table, the energy difference among the HL-B2-3, HL-B2-1 and HL-B1-3 configurations are only 30 meV, which is in the range of the inherent error of DFT. Therefore, they are all energetically favorable for coadsorption of H and CH_3, in which the atomic H and CH_3 species are adsorbed at the Hollow and Bridge site, respectively. In addition, the H atoms in the B-B2-2 and B-B2-3 configurations are relaxed to the Hollow sites even if initially placed at the Bridge sites, i.e., the B-B2-2 and B-B2-3 configuration are optimized to the HL-B2-3 and HL-B2-1 configuration, respectively. It is therefore evident that the interaction between the coadsorbed CH_3 and H is repulsive.

The mode softening is also observed as H and CH_3 are coadsorbed on Ni(1 0 0) surface, e.g., as for the HL-B2-3 configuration, the "soft" frequency of the C–H symmetric stretching occurs at ~2631 cm^{-1}.

3.4. CH_4 adsorption and dissociation on Ni(1 0 0) surface

3.4.1. CH_4 adsorption on Ni(1 0 0) surface

The CH_4 adsorptions at the Hollow, Bridge and Atop sites of Ni(1 0 0) surface are also studied. At each site, different adsorption configurations are considered with one, two and three C–H bonds in CH_4 species pointing towards Ni(1 0 0) surface, as shown in Fig. 7. The adsorption energies which are calculated relative to the bare Ni(1 0 0) surface and isolated CH_4 molecule are summarized in Table 4, together with the optimized geometry parameters. Because the nature of the interaction between CH_4 and Ni surface is physisorption, not only the ZPE but also the dispersion energy is added to the total energy. For all of these adsorption configurations, the adsorption energies takes similar small values in the range of a few meV and in the most stable 1-A-1 and 1-A-2 adsorption configurations, one C–H bond in the CH_4 molecule points directly towards the Atop site and the remaining three H atoms are in a plane parallel to the Ni surface. Öström et al. performed combined X-ray absorption spectroscopy (XAS) and DFT studies to investigate the CH_4 physisorption on Pt surfaces [45]. They found that the CH_4 molecule with one H atom pointing towards the surface resulted in more satisfactory agreement with the experimental spectra and this C–H bond was elongated, which induced the orbital mixing and consequently minimized the Pauli repulsion. In addition, the CH_4 diffusion above Ni(1 0 0) surface is calculated and the energy barrier for CH_4 rotation from the 1-A-1 configuration to the 1-A-2 configuration is negligible.

3.4.2. CH_4 dissociation on Ni(1 0 0) surface

Now that the stable sites for CH_4 adsorption and coadsorption of H and CH_3 have been established, the CI-NEB method is used to explore the MEP for CH_4 dissociation. Three reaction pathways with different initial and final states have been conducted to investigate the effect of the CH_4 orientation on reactivity. As mentioned in the CH_4 adsorption, the CH_4 orientations with one, two and three C–H bonds pointing towards the Ni surface are considered. For clarity and ease of notation, these three reaction pathways are denoted as PATH(I), PATH(II), and PATH(III), respectively. In the PATH(I), the initial state adopts the favorable 1-A-1 configuration for CH_4 adsorption and the final state adopts the stable HL-B2-3 configuration for the coadsorbed H and CH_3 as described above. The result of

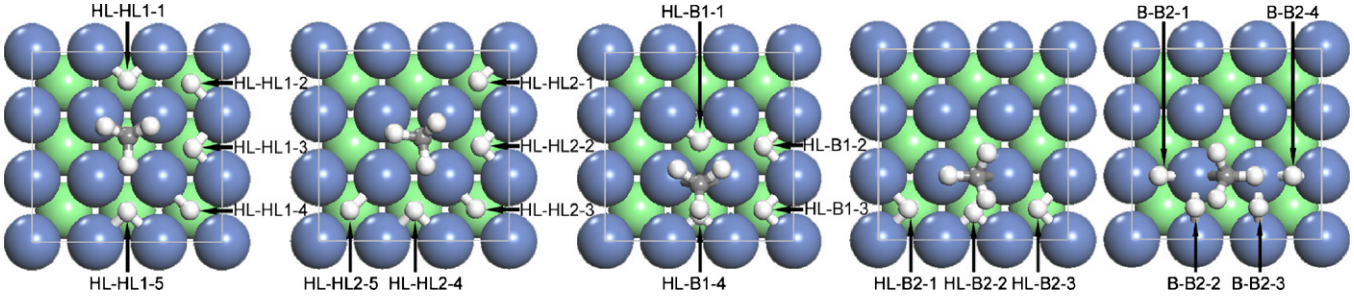

Fig. 6. Schematic representations of geometries of coadsorbed H and CH_3 on Ni(1 0 0) surface. The first character in the name of coadsorption configurations refers to the adsorption site for atomic H. The character after the first hyphen refers to the CH_3 adsorption configuration. HL denotes Hollow and B denotes Bridge.

Table 3
Adsorption energies and geometries of coadsorbed CH_3 and H on Ni(1 0 0) surface

Configuration	ΔE_{ads} (eV)		$d_{C–Ni}$ (Å)	$d_{C–surface}$ (Å)	$d_{H–Ni}$[a] (Å)	$d_{H–surface}$[b] (Å)	∠HCH (°)	$d_{C–H}$ (Å)
	Uncorrected[c]	Corrected						
HL-HL1-1	−4.46	−4.51	2.135 (2)	1.478	1.744 (2)	0.507	104.911, 104.932 (2)	1.121 (2), 1.125
HL-HL1-2	−4.61	−4.65	2.049	1.541	1.821	0.556	104.998, 105.733, 106.284	1.120, 1.121, 1.122
HL-HL1-3	−4.61	−4.64	2.030	1.602	1.776	0.558	105.644, 106.515, 107.121	1.114, 1.116, 1.119
HL-HL1-4	−4.59	−4.64	2.069	1.474	1.784	0.604	104.882, 105.380, 105.508	1.114, 1.121, 1.128
HL-HL1-5	−4.69	−4.72	2.054 (2)	1.688	1.815 (2)	0.568	104.832, 108.285 (2)	1.102, 1.118 (2)
HL-HL2-1	−4.65	−4.69	1.994	1.526	1.773	0.558	102.324, 105.648 (2)	1.107, 1.132 (2)
HL-HL2-2	−4.58	−4.62	2.019	1.558	1.744	0.533	102.912, 105.435, 106.512	1.109, 1.123, 1.138
HL-HL2-3	−4.67	−4.72	1.994	1.499	1.814	0.570	101.590, 105.479, 105.709	1.105, 1.134, 1.137
HL-HL2-4	−4.65	−4.68	1.983	1.619	1.799	0.545	103.771, 106.094, 107.692	1.107, 1.116, 1.132
HL-HL2-5	−4.66	−4.70	1.992	1.507	1.798	0.600	101.986, 105.849 (2)	1.105, 1.135 (2)
HL-B1-1	−4.41	−4.42	2.080 (2)	1.821	1.707 (2)	0.192	103.284, 110.145 (2)	1.109, 1.115 (2)
HL-B1-2	−4.68	−4.67	2.050	1.789	1.799	0.516	109.508, 109.614, 109.787	1.099, 1.110, 1.116
HL-B1-3	−4.71	−4.73	2.050	1.800	1.803	0.541	103.954, 109.591, 109.695	1.098, 1.113, 1.115
HL-B1-4	−4.28	−4.28	2.101 (2)	1.886	1.697 (2)	0.135	105.147, 110.046 (2)	1.095, 1.109 (2)
HL-B2-1	−4.73	−4.74	1.994	1.764	1.789	0.530	104.869, 105.364, 111.164	1.097, 1.110, 1.131
HL-B2-2	−4.44	−4.46	2.012	1.817	1.711	0.219	104.032, 105.793, 110.707	1.097, 1.106, 1.137
HL-B2-3	−4.74	−4.76	2.005	1.781	1.781	0.552	104.497, 104.641, 110.987	1.099, 1.101, 1.141
B-B2-1	−4.60	−4.61	2.012	1.792	1.591	1.116	104.520 (2), 110.726	1.099 (2), 1.150
B-B2-2	−4.73	−4.75	2.017	1.808	1.796	0.615	103.237, 105.005, 110.693	1.099, 1.102, 1.145
B-B2-3	−4.73	−4.74	1.983	1.794	1.811	0.571	103.810, 105.911, 110.681	1.100, 1.103, 1.137
B-B2-4	−4.54	−4.54	1.967	1.821	1.567	1.107	104.937 (2), 111.258	1.100 (2), 1.133

[a] $d_{H–Ni}$ denotes the shortest distance between the dissociated H atom and Ni atoms.
[b] $d_{H–surface}$ denotes the height of the isolated H atom above the surface.
[c] The uncorrected adsorption energy is calculated as $\Delta E_{ads} = E_{CH_3+H+Ni(1\,0\,0)} - E_{CH_3} - E_H - E_{Ni(1\,0\,0)}$.

this calculation is depicted in Fig. 8. The energy barrier for CH_4 dissociation is found to be 0.84 eV. With the ZPE and dispersion energy correction considered, the barrier is decreased to 0.61 eV which is much lower than that calculated by Lai et al. [20] (0.73 eV) and closer to the experimental data by Nielsen et al. [6] (0.61 ± 0.02 eV). Through the frequency analysis, the transition state has been verified with only one imaginary vibrational frequency of 671.18i cm^{-1} which corresponds to an asymmetric stretching. At the saddle point (Fig. 8(b)), one H atom is moved to the Bridge site and the remaining CH_3 species is still located at the Atop site. The C–Ni bond forms angles of 0.841° and 48.591° with respect to the surface normal and the dissociating C–H bond, respectively. The length of the dissociating C–H bond is stretched from the value of 1.097 Å in the isolated CH_4 molecule to 1.626 Å. The underlying Ni atom is displaced out of the surface along the surface normal by 0.251 Å. This phenomenon has also been proposed in calculation of CH_4 dissociation on Ir(1 1 1) [31] and Ni(1 1 1) surfaces [22] and can be explained on the basis of shifts in the metal d band induced by stress [46]. The Ni displacement results in the decrease of coordination number, and consequently the higher d-band center to enhance the reactivity.

In the PATH(II), the 2-A configuration is chosen as the reactant with two C–H bonds pointing toward the Ni surface and the

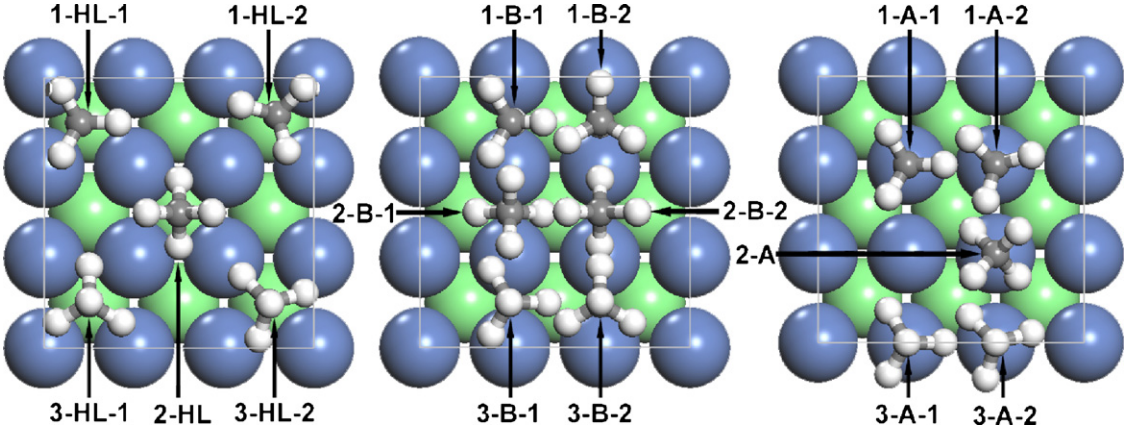

Fig. 7. Schematic representations of CH_4 adsorption at three high-symmetry sites of Ni(1 0 0) surface with different orientations. Small white balls denote H atoms, and small grey balls denote C atoms. The first character in the name of adsorption configurations refers to the number of H atoms pointing towards the Ni surface. The character after the first hyphen refers to where the CH_4 molecule is adsorbed. HL denotes Hollow. B denotes Bridge. A denotes Atop.

Table 4
Adsorption energies and optimized geometries of CH_4 adsorption on Ni(1 0 0) surface

Configuration	ΔE_{ads} (eV)		$d_{C–Ni}$ (Å)	$d_{C–surface}$ (Å)	$d_{C–H}$[a] (Å)	∠HCH[b] (°)
	Uncorrected[c]	Corrected[d]				
1-HL-1	0.06	0.04	3.502 (2)	3.095	1.095 (2), 1.096, 1.109	108.120, 108.478 (2), 110.528 (2), 110.626
1-HL-2	−0.01	−0.01	3.661	3.362	1.096 (2), 1.098, 1.105	108.800 (2), 108.863, 110.073 (2), 110.195
2-HL	0.04	0.02	3.528 (4)	3.048	1.096 (2), 1.104 (2)	108.516, 109.355 (4), 110.869
3-HL-1	0.04	0.03	3.426 (2)	2.920	1.093, 1.097, 1.098 (2)	109.093 (2), 109.145, 109.779, 109.856 (2)
3-HL-2	0.09	0.06	3.306	2.779	1.096, 1.102 (2), 1.103	108.764, 108.774 (2), 110.086 (2), 110.316
1-B-1	0.04	0.01	3.361 (2)	3.111	1.095 (2), 1.097, 1.113	108.066, 108.281 (2), 110.503, 110.804 (2)
1-B-2	0.01	−0.01	3.430	3.211	1.081, 1.096 (2), 1.118	107.935 (2), 108.512, 110.545, 110.896 (2),
2-B-1	0.07	0.05	3.232 (2)	2.964	1.099 (2), 1.104 (2)	109.169 (4), 109.204, 110.937,
2-B-2	0.08	0.05	3.064 (2)	2.785	1.096 (2), 1.108 (2),	108.744 (4), 109.892, 110.960
3-B-1	0.01	0.00	3.308 (2)	3.059	1.095, 1.097, 1.098 (2)	108.973, 109.463 (2), 109.561 (2), 109.802
3-B-2	0.01	0.00	3.353	3.107	1.096 (2), 1.098, 1.099	109.098 (2), 109.407, 109.714, 109.754 (2)
1-A-1	−0.04	−0.05	3.751	3.754	1.096 (3), 1.101	109.066, 109.120 (2), 109.837 (2), 109.839
1-A-2	−0.04	−0.05	3.751	3.754	1.097 (3), 1.101	109.106, 109.143 (2), 109.791 (2), 109.847
2-A	−0.01	−0.02	3.151	3.162	1.102 (2), 1.097 (2)	109.128 (4), 109.549, 110.764
3-A-1	0.00	−0.01	3.149	3.151	1.097, 1.098 (2), 1.099	109.336 (2), 109.400, 109.564, 109.596 (2)
3-A-2	0.00	−0.01	3.151	3.151	1.095, 1.099 (3)	109.338 (2), 109.398, 109.565, 109.594 (2)

[a] d_{C-H} denotes the lengths of C–H bonds in CH_4 species.
[b] ∠HCH denotes the angles between the C–H bonds in CH_4 species.
[c] The uncorrected adsorption energy is calculated as $\Delta E_{ads} = E_{CH_4+Ni(1\,0\,0)} - E_{CH_4} - E_{Ni(1\,0\,0)}$.
[d] The corrected adsorption energy is calculated with both the ZPE and dispersion energy correction considered.

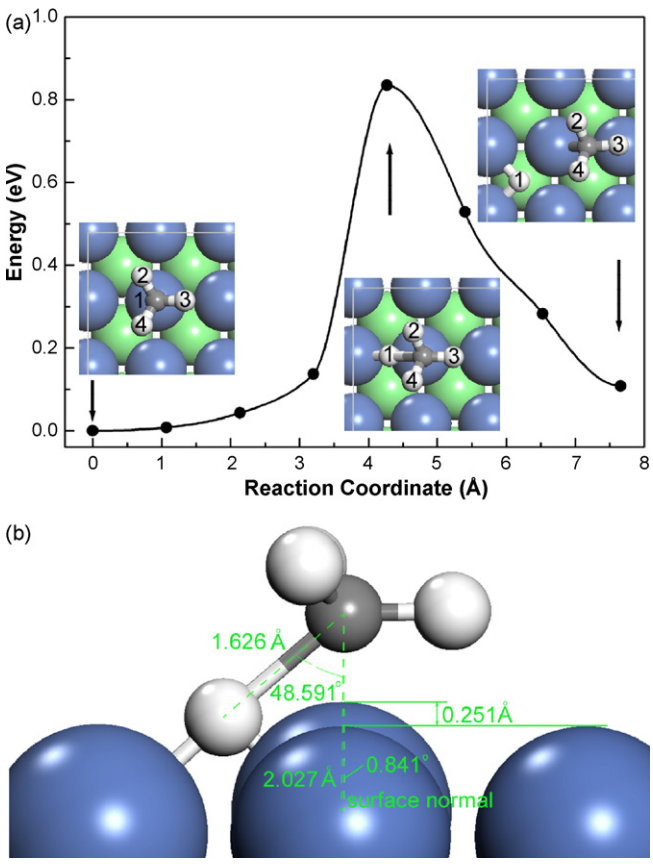

Fig. 8. (a) MEP for CH_4 dissociation adopting the PATH(I) with the initial state, the transition state and the final state illustrated. (b) Geometry of the saddle point for CH_4 dissociation.

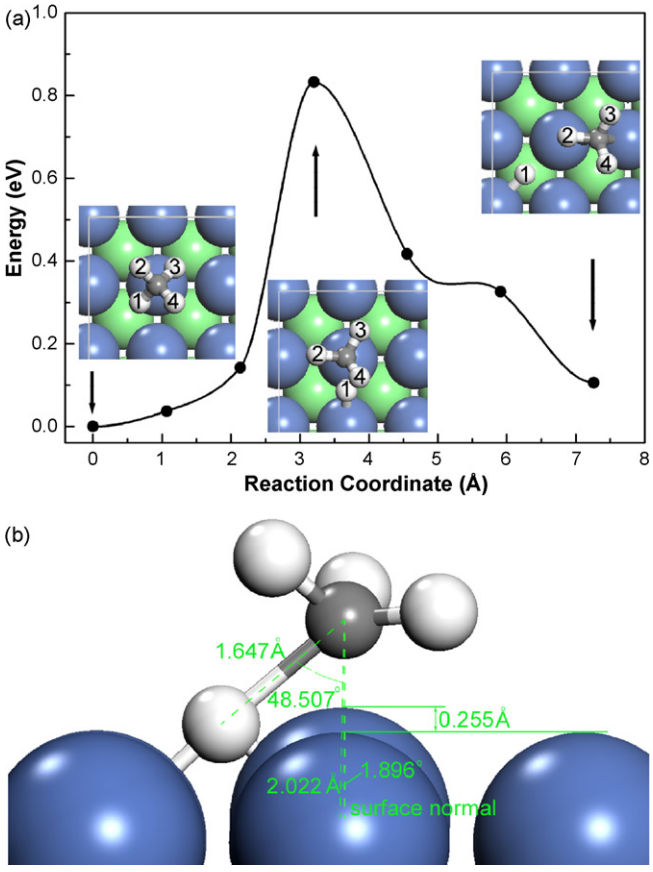

Fig. 9. (a) MEP for CH_4 dissociation adopting the PATH(II) with the initial state, the transition state and the final state illustrated. (b) Geometry of the saddle point for CH_4 dissociation.

HL-B2-1 configuration is selected as the product. The calculated MEP is presented in Fig. 9(a) with the initial state, the transition state and the final state shown in the insets from the left to the right. The data along the energy profile yields a dissociation barrier of 0.83 eV. Considering the ZPE and dispersion energy correction, this value is decreased to 0.61 eV which is identical with that for PATH(I). Through the frequency analysis, the transition state has been verified with only one imaginary vibrational frequency of $620.91i\,cm^{-1}$. What is beyond our expectation is that the dissociated H atom is not directly moved to the Hollow site to form the C–H–Ni bond. Instead, it firstly diffuses to the Bridge site to achieve the maximum three-center bonding to lower the energy barrier and then diffuses to the Hollow site. Fig. 9(b) shows the corresponding geometry of the saddle point along the MEP. The C–Ni bond forms angles of 1.896° and 48.507° with respect to the surface normal and the dissociating C–H bond, respectively, and the dissociating C–H bond is stretched to 1.688 Å. The underlying Ni atom is displaced out of the surface along the surface normal by 0.255 Å.

In the PATH(III) starting from the CH_4 molecule with three C–H bonds pointing towards the Ni surface, the initial and final states correspond to the 3-A-1 and B-B2-4 configurations, respectively. The converged MEP and the corresponding geometry of the transition state are shown in Fig. 10. As seen in this figure, the calculated energy barrier is 0.84 eV, and the corrected result is 0.62 eV which is slightly higher than those for PATH(I) and PATH(II). There is only one vibrational imaginary frequency of $554.05i\,cm^{-1}$ in the transition state. The geometry of the saddle point is similar to that in PATH(I) except that the dissociating CH_3 is rotated through 180° about the surface normal going through the C atom. The C–Ni bond forms angles of 1.593° and 48.363° with respect to the surface normal and dissociating C–H bond, respectively. The length of the dissociating C–H bond is stretched to 1.688 Å and the underlying Ni atom is displaced out of the surface along the surface normal by 0.267 Å.

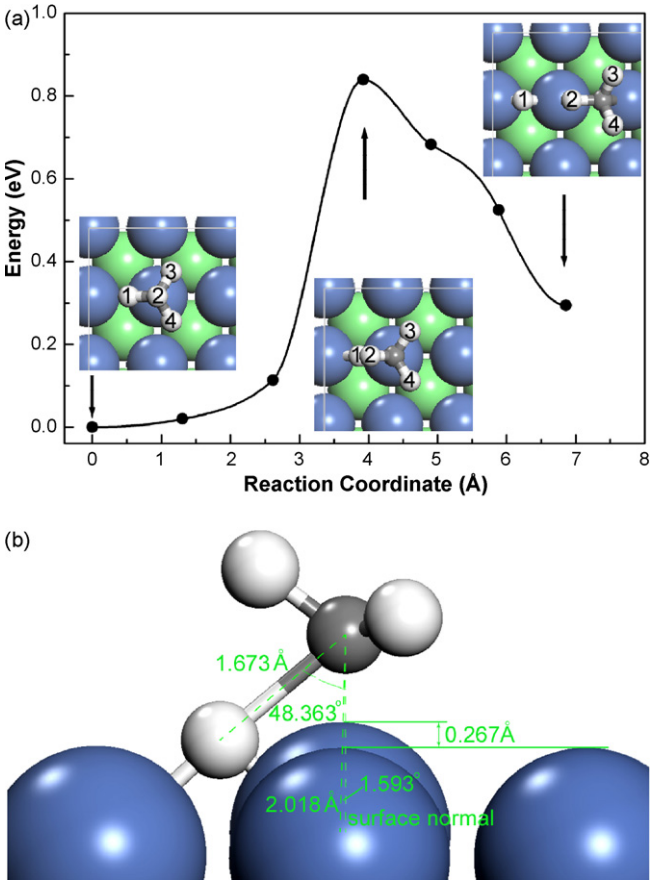

Fig. 10. (a) MEP for CH4 dissociation adopting the PATH(III) with the initial state, the transition state and the final state illustrated. (b) Geometry of the saddle point for CH_4 dissociation.

Through the investigation of these three reaction pathways, the activation energies take similar values so the CH_4 orientation has a minor effect on the reactivity of the CH_4 dissociation. In the transition states, the C–H–Ni three-center bonds are formed and they can substantially lower the energy barrier for CH_4 dissociation.

4. Conclusions

Density functional theory calculations have been performed to study the adsorption of H, CH_3 and CH_4 on Ni(1 0 0) surface. The fourfold Hollow site is most favorable for H adsorption, while the CH_3 species prefers the Bridge site with one of the C–H bonds pointing towards the neighbor Ni atom. The C–H–Ni three-center bond is formed as CH_3 is adsorbed on Ni surfaces. The Bridge2 configuration is most stable for CH_3 adsorption because it achieves the maximum multicenter bonding. Because of a weakening of the 2a1–3d delocalization and 1e–3d mixing, the Atop site is less favorable although the corresponding C–Ni covalent bond is strongest. The three-center bond results in a shortened H–Ni distance and a lengthened C–H bond. Consequently, a mode softening in CH_3 species is observed due to the weakened C–H bond. The CH_3 diffusion on Ni(1 0 0) surface is investigated using the CI-NEB method with the CH_3 species adopting the most stable Bridge2 configuration in both the initial and final states. Unlike the CH_3 rotation from the Fcc site to other adsorption sites on Ni(1 1 1) surface, the CH_3 rotation on Ni(1 0 0) surface is constrained at the Bridge site throughout the diffusion with a much smaller energy barrier of 28 meV. The different behaviors of CH_3 on Ni(1 0 0) and Ni(1 1 1) surfaces are also due to the strong three-center bond. Several configurations are favorable for the coadsorption of the atomic H and CH_3 species, in which the H atom and CH_3 species are adsorbed at the Hollow and Bridge site, respectively, because of their little energy difference.

Three reaction pathways starting from different CH_4 orientations have been explored to investigate the CH_4 dissociation using the CI-NEB method. The three CH_4 orientations correspond to the CH_4 molecules with one, two and three C–H bonds pointing towards the Ni surface. The calculated dissociation energy barriers are 0.61, 0.61 and 0.62 eV, respectively, consistent with the experimental result of 0.61 ± 0.02 eV. Because the energy barriers for the different reaction pathways take similar values, the CH_4 orientation has a minor effect on the reactivity. In the transition states, the active Ni atoms are displaced out of the surface to decrease the coordination number and enhance the

reactivity, and simultaneously the energy barrier for dissociation is lowered by the formed C–H–Ni three-center bonds.

The validity of the present set of results is restricted to the case of a perfect Ni surface without defective sites. As this is clearly an approximation of the Ni surface, investigations to address the influence of the surface defective sites upon the chemisorption and reaction properties of CH_4 molecule should also be considered in the future.

Acknowledgements

We thank Dr. Xinggui Zhou, Ping Li, Jinghong Zhou, Xiongyi Gu, Tiejun Zhao and Zhijun Sui for valuable discussions. This work is supported by NSFC/PetroChina through a major project on multiscale methodology (No. 20490200).

References

[1] J.R. Rostrup-Nielsen, in: J.R. Anderson, M. Boudart (Eds.), Catalysis, Science and Technology, vol. 5, Springer, Berlin, 1984, p. 1.
[2] N.M. Rodriguez, J. Mater. Res. 8 (1993) 3233.
[3] K.P. De-Jong, J.W. Geus, Catal. Rev. Sci. Eng. 42 (2000) 481.
[4] A.C. Luntz, J. Harris, Surf. Sci. 258 (1991) 397.
[5] R.T. Yang, J.P. Chen, J. Catal. 115 (1989) 52.
[6] B.O. Nielsen, A.C. Luntz, P.M. Holmblad, I. Chorkendorff, Catal. Lett. 32 (1995) 15.
[7] R.C. Egeberg, S. Ullmann, I. Alstrup, C.B. Mullins, I. Chorkendorff, Surf. Sci. 497 (2002) 183.
[8] C.T. Rettner, H.E. Pfnür, D.J. Auerbach, Phys. Rev. Lett. 54 (1985) 2716.
[9] M.B. Lee, Q.Y. Yang, S.T. Ceyer, J. Chem. Phys. 87 (1987) 2724.
[10] P.M. Holmblad, J. Wambach, I. Chorkendorff, J. Chem. Phys. 102 (1995) 6255.
[11] V.A. Ukraintsev, I. Harrison, J. Chem. Phys. 101 (1995) 1564.
[12] R.D. Beck, P. Maroni, D.C. Papageorgopoulos, T.T. Dang, M.P. Schmid, T.R. Rizzo, Science 302 (2003) 98.
[13] P. Maroni, D.C. Papageorgopoulos, M. Sacchi, T.T. Dang, R.D. Beck, T.R. Rizzo, Phys. Rev. Lett. 94 (2005) 246104.
[14] L.B.F. Juurlink, P.R. Mccabe, R.P. Smith, C.L. Dicologero, A.L. Utz, Phys. Rev. Lett. 83 (1999) 868.
[15] L.B.F. Juurlink, R.P. Smith, D.R. Killelea, A.L. Utz, Phys. Rev. Lett. 94 (2005) 208303.
[16] R. Milot, A.P. Jansen, J. Phys. Rev. B 61 (2000) 15657.
[17] H.L. Abbott, A. Bukoski, D.F. Kavulak, I. Harrison, J. Chem. Phys. 119 (2003) 6407.
[18] O.K. Swang Jr., O. Faegri, U. Gropen, P. Wahlgren, Siegbahn, Chem. Phys. 156 (1991) 379.
[19] H.S. Bengarrd, I. Alstrup, I. Chorkendorff, S. Ullmann, J.R. Rostrup-Nielsen, J.K. Nørskov, J. Catal. 187 (1999) 238.
[20] W.Z. Lai, D.Q. Xie, D.H. Zhang, Surf. Sci. 594 (2005) 83.
[21] P. Kratzer, B. Hammer, J.K. Nørskov, J. Chem. Phys. 105 (1996) 5595.
[22] G. Henkelman, A. Arnaldsson, H. Jónsson, J. Chem. Phys. 124 (2006) 044706.
[23] G. Kresse, J. Hafner, Phys. Rev. B 48 (1993) 13115.
[24] G. Kresse, J. Furthmüller, Comp. Mater. Sci. 6 (1996) 15.
[25] G. Kresse, J. Furthmüller, Phys. Rev. B 54 (1996) 11169.
[26] P.E. Blöchl, Phys. Rev. B 50 (1994) 17953.
[27] J.P. Perdew, K. Burke, M. Ernzerhof, Phys. Rev. Lett. 77 (1996) 3865.
[28] H.J. Monkhorst, J.D. Pack, Phys. Rev. B 13 (1976) 5188.
[29] M. Methfessel, A.T. Paxton, Phys. Rev. B 40 (1989) 3616.
[30] G. Kresse, J. Hafner, Surf. Sci. 459 (2000) 287.
[31] G. Henkelman, H. Jónsson, Phys. Rev. Lett. 86 (2001) 664.
[32] S. Kristyán, P. Pulay, Chem. Phys. Lett. 229 (1994) 175.
[33] S. Tsuzuki, T. Uchimaru, M. Mikami, K. Tanabe, J. Phys. Chem. A 106 (2002) 3867.
[34] R.W. Williams, D. Malhota, Chem. Phys. 327 (2006) 54.
[35] G.C. Maitland, M. Rigby, E.B. Smith, W.A. Wakeham, Intermolecular Forces, Clarendon Press, Oxford, 1981, p. 63.
[36] H. Jónsson, G. Mills, K.W. Jacobsen, in: B.J. Beren, G. Ciccitti, D.F. Coker (Eds.), Classical and Quantum Dynamics in Condensed Phase Simulations, World Scientific, Singapore, 1998, p. 385.
[37] G. Henkelman, B.P. Uberuaga, H. Jónsson, J. Chem. Phys. 113 (2000) 9901.
[38] G. Henkelman, H. Jónsson, J. Chem. Phys. 113 (2000) 9978.
[39] R.G. Della-Valle, H.C. Andersen, J. Chem. Phys. 97 (1992) 2682.
[40] G. Henkelman, H. Jónsson, J. Chem. Phys. 111 (1999) 7010.
[41] S.T. Ceyer, J.D. Beckerle, M.B. Lee, S.L. Tang, Q.Y. Yang, M.A. Hines, J. Vac. Sci. Technol. A 5 (1987) 501.
[42] M.B. Lee, Q.Y. Yang, S.T. Ceyer, J. Chem. Phys. 87 (1987) 2724.
[43] K. Christmann, R.J. Behm, G. Ertl, J. Chem. Phys. 70 (1979) 4168.
[44] A. Michaelides, P. Hu, Surf. Sci. 437 (1999) 362.
[45] H. Öström, H. Ogasawara, L. Näslund, L.G.M. Pettersson, A. Nilsson, Phys. Rev. Lett. 96 (2006) 146104.
[46] M. Mavrikakis, B. Hammer, J.K. Nørskov, Phys. Rev. Lett. 81 (1998) 2819.